water

MDPI

Article

On the Effect of Regular Waves on Inclined Negatively Buoyant Jets

Simone Ferrari, Maria Grazia Badas and Giorgio Querzoli *

Dipartimento di Ingegneria Civile, Ambientale e Architettura (DICAAR), University of Cagliari, via Marengo 2, 09123 Cagliari, Italy; ferraris@unica.it (S.F.); mgbadas@unica.it (M.G.B.)
* Correspondence: querzoli@unica.it; Tel.: +39-070-675-5308

Received: 28 February 2018; Accepted: 31 May 2018; Published: 3 June 2018

Abstract: The target of this paper is to measure the modifications that regular waves induce on the geometrical features and dilution of inclined negatively buoyant jets. In order to achieve this aim, we have carried out a set of experiments in a wavemaker-equipped flume, by measuring the concentration fields via light-induced fluorescence, a non-intrusive and full-field image analysis technique. The wave and jet parameters were selected in order to simulate the case of a typical discharge of brine, from a desalination plant, into the Mediterranean Sea, and compare it to a reference case, i.e., the same jet discharging into a stagnant water body. The mean concentration fields were obtained, as well as the geometrical features and dilution of the jets. The three main effects of waves on inclined negatively buoyant jets are the bifurcation (i.e., the separation in two branches), the rotation of the point of maximum height and the oscillation of the impact point around a fixed position different from the stationary one, and the reduction in size of the sea region interested by the discharge; this last effect increases with the wave period. As a consequence, under waves with high period and amplitude, the dilution of inclined negatively buoyant jets tends to decrease.

Keywords: inclined negatively buoyant jets; regular waves; dilution; sea discharges

1. Introduction

A negatively buoyant jet (NBJ) is the phenomenon that develops when a fluid is discharged, with a non-negligible momentum, in a less dense fluid. As the jet tends to fall downwards, it is typically released upwards, with a certain angle to the horizontal, in order to increase the path length and, consequently, the final dilution. Due to the several practical applications of inclined NBJs (see Ferrari and Querzoli, 2010 [1], for a list), many researches during the last few years focused on this topic.

In particular, many experimental investigations on NBJs released into a stationary receiving body can be found in recent years. Qiao et al. (2017, [2]) carried out an experimental and theoretical study on the internal hydraulics of NBJs from diffusers for sewage disinfection. Bashitialshaaer et al. (2012, [3] and 2015, [4]), measured in a laboratory model the geometrical features and the dilution of inclined NBJs. Seo and Song (2015, [5]) tested the influence of different diffuser types on the dispersion of NBJs for the particular application of the discharge of cooled water. Christodoulou et al. (2015, [6]) focused on the achieved dilution at the impact point and on its dependence on the NBJ inclination and on the densimentric Froude number. Oliver et al. (2013, [7]) removed the bottom boundary to find dilutions not affected by the stratification of dense effluent at the bottom. Geyer et al. (2012, [8]) experimentally obtained a chart of the dependence of flow types on Richardson, Reynolds and Weber numbers. Papakonstantis et al. (2011-a [9] and 2011-b [10]) experimentally studied the geometrical characteristics (via image analysis techniques) and the concentration (via probes) of inclined NBJs. In other experiments, velocity measurements were performed (e.g., Crowe et al., 2012 [11] and 2016 [12],

Besalduch et al., 2013 [13] and 2014 [14]), highlighting, among the other results, the different turbulent quantities in the upper and lower boundaries of NBJs.

The number of experimental investigations on the discharge of NBJs into a non-stationary receiving body are much less. Malcangio et al., 2016 [15], studied in the laboratory the turbulent features of vertical buoyant jets discharged into a transversal current. Hajikandi and Barjastehmaleki (2015, [16]) and Lai and Lee (2014, [17]) experimentally studied the mixing of inclined NBJs discharged into, respectively, a co-flow and a perpendicular cross-flow. Yang et al. (2005, [18]) experimentally investigated NBjs with a different angle discharged in a cross flow. Davies et al. (2001, [19]) and Davies and Ahmed (1996, [20]) studied, with both laboratory and numerical simulations, the peculiar case of an NBJ discharged horizontally into a rotating homogeneous fluid. Moreover, Stancanelli et al. (2018, [21]), experimentally investigated a buoyancy current in the presence of regular waves.

Regarding the jets released into a wave environment, some experimental researches on horizontal NBJs, on positively buoyant jets and on simple jets can be found in the literature. Bas et al. (2012, [22]) focused their experiments on the effect of the wave direction (discharge in the wave direction or in the opposite direction) on the dilution of horizontal NBJ. They found a higher dilution for the discharge in the opposite direction to the wave propagation, compared to both the dilution obtained in a stagnant receiving environment and the dilution of the co-flow discharge. Lin et al. (2011, [23]), investigated experimentally the turbulent properties of horizontal NBJs and non-buoyant jets under regular progressive waves via Particle Image Velocimetry (PIV). They found that dilution is increased by the wave motion. The same authors (Lin et al. 2013, [24]) measured, via PIV, the mean velocity and turbulence properties in a horizontal (positively, neutrally and negatively) buoyant jet discharged in the opposite direction to the wave propagation. They found that the width and the dilution of the positively and negatively buoyant jets increased in the wave receiving environment. Also Chin (1987, [25]) and Sharp (1986, [26]) observed experimentally that the dilution of a buoyant jet in a wave environment is significantly higher than in a stagnant one.

Many other Authors found similar results about the increased dilution due to the larger spreading caused by waves also on simple jets (e.g., Xu et al., 2016-a [27] and 2016-b [28], Hsiao et al., 2011 [29], Chang et al., 2009 [30], Ryu et al., 2005 [31], Mossa, 2004 [32], Chyan and Hwung, 1993 [33], Chyan et al., 1991 [34]). In this context, the classification formulated by Chyan and Hwung (1993, [33]) for the regions of a jet interacting with waves is particularly relevant: They identified three regions, namely the jet deflection region, the transition region and the developed jet region. In the jet deflection region, the jet still has most of its initial momentum and so it tends to preserve its shape; the influence of the wave on the jet deflection region is consequently an oscillation of the jet around its stationary position. This behavior has been confirmed by the experiments of Mossa (2004, [32]), Chyan et al. (1991, [34]) and Sharp (1986, [24]): They have shown that this oscillation has a considerable effect on the jet dilution. In the developed jet region, a periodic deflection, observed by Chyan and Hwung (1993, [31]) and Chin (1987, [26]), was found to be one of the main reasons for the higher dilution reached by a jet released in the presence of waves.

Although the increase of the dilution of a jet has been measured in many experimental investigations, to the best of the authors' knowledge the effects of regular waves on inclined (not horizontal or vertical) NBJs were never investigated before. For this reason, Ferrari and Querzoli, 2015 [35], performed a preliminary series of experiments that highlighted significant differences among the behavior of simple or positively buoyant jets and the case of the inclined negatively buoyant jets. As a consequence, a new set of carefully designed experiments were performed, with the main aim of better characterizing the peculiar behavior of negatively buoyant jets in a wavy environment and, in particular, of measuring the changes in the most important parameter for the design of environmentally friendly sea outfalls, i.e., the achieved dilution. In the present paper we present the results arising from this new set of experiments.

This paper is structured as follows: In Section 2, the experimental set-up, the run parameters and the data elaboration are briefly described; in Section 3, the results are shown and discussed; in Section 4, the conclusions are drawn.

2. Materials and Methods

The experimental set-up simulates a typical configuration of a submarine outfall, i.e., the discharge from an orifice in the lateral wall of a pipe laid down on the sea bottom. A solution of water, sodium-sulphate and fluorescein was released, through a sharp-edged orifice outlet with a diameter $D = 4.0$ mm and an angle to the horizontal $\theta = 67°$, into a flume with glass walls. The solution came from a constant head tank to a cylindrical pipe with a 25.0 mm diameter. The sodium-sulphate was employed to increase the density of the solution, the fluorescein to allow concentration measurements via a Light Induced Fluorescence (LIF) technique (a non-intrusive and full-field image analysis technique). The flume is 21.00 m long and 0.30 m wide and it is equipped with a piston-type wavemaker, on one side, and an absorbing beach, on the opposite side, to minimize the reflections. The wavemaker can produce monochromatic or random waves. The water depth d was kept constant at 0.40 m.

The key parameter controlling the behavior of negatively buoyant jets is the densimetric Froude number Fr:

$$Fr = \frac{U}{\sqrt{\frac{gD(\rho_D - \rho_R)}{\rho_R}}} \tag{1}$$

where U is the outlet mean velocity, g the gravitational acceleration, ρ_D the discharged fluid density and ρ_R the receiving fluid density. The Reynolds number is defined here as $Re = UD/\upsilon$, where υ is the kinematic viscosity of the discharged fluid. Two sets of experiments were performed, with Fr equal to 18.0 and 28.0, and a Re of 10^3 (higher than the critical value of around 500 for the present set-up, as shown by Ferrari and Querzoli, 2010 [1]) and five monochromatic waves, with wave periods T of 0.50 s, 1.00 s and 1.50 s (corresponding to wave lengths L of 0.39 m, 1.56 m and 3.51 m) and wave amplitudes A of 5.00 mm and 12.50 mm (see Table 1). A reference run with a NBJ released in a stagnant environment was performed for each Fr. The ratio of the water depth d to the wave length L was in the deep-water regime ($d/L = 1.02$) or in the intermediate-depth water regime ($d/L = 0.26$ and 0.11); the ratio between the wave height $H = 2A$ and L was between 0.003 and 0.026, typical values of a long wave. The experimental set-up dimensions and wave parameters were chosen in order to simulate a typical submerged discharge in the Mediterranean Sea, with respect to the geometrical similarity (scale model $K_L = L_M/L_P = 1/40$; the subscript M stands for Model and the subscript P for Prototype), to the kinematic similarity and to the dynamic (Froude) similarity, achieved through the respect of the following equations (see e.g., Von Ellenrieder and Dhanak, 2016 [36]):

$$A_M = A_P K_L, \tag{2}$$

$$T_M = T_P \sqrt{K_L}. \tag{3}$$

In Figure 1, the data of the wave period, T, versus the wave height H recorded by the Alghero wave buoy (in the north-western sea of Sardinia) of the RON—Rete Ondametrica Nazionale (Italian national wavemetric system [37]) from 2002 to 2014 are shown. These data were employed to define the wave parameters of the present experiments. As a matter of fact, by using Equations (2) and (3), the simulated prototype waves have $H = 2A = 0.40 - 1.00$ m and $T = 3.16 - 6.32 - 9.49$ s, hence their values are within the range of those registered by the Alghero wave buoy.

The jet is discharged rightwards, in the opposite direction to the wave propagation and the flume is long enough to avoid an accumulation of dense fluid on the bottom during the duration of the experiment.

The axial vertical jet section was illuminated by a light sheet and a 3-CCD video-camera placed orthogonal to the light sheet. The experiments were recorded with a frame rate of 25 fps, a resolution

of 720 × 576 pixels and a bit depth of 8 bit per color. As a consequence, the recorded images showed a bright jet on a dark background and, as the fluorescein concentration was very low, a linear relationship between the light intensity and the salt concentration holds true (Troy and Kosseff, 2005 [38], Sutton et al., 2008 [39]), so we used light intensity as a proxy for the salt concentration.

The free surface levels were measured via the image analysis technique developed by Ferrari et al., 2016 [40]; the framed zone for the wave height measurement had a spatial resolution of around 11.62 px/mm, so the 10 mm height wave was measured with a resolution of around ±0.86% and the 25 mm height wave with a resolution of around ±0.34%. The resolution in the concentration measurements is around 0.4%. The resolution on the measured distances (*X/D* and *Y/D*) depends on the spatial resolution of the investigation area, which is not the same for every experiment and varies from a minimum of 14.26 px/cm (run 7) to 20.89 px/cm (run 6). In addition, following Bendat and Piersol, 2010 [41], the uncertainty of the statistics presented in this paper was estimated from their standard deviation and was then computed over all the recorded images for each experiment (5000 for T = 0.5 s, 10000 for T = 1.0 s, 15,000 for T = 1.5 s); the maximum uncertainty varies from a minimum of 3.35% (run 3) to a maximum of 4.52% (run 8).

Table 1. Main parameters for the experiments; *A* is the wave amplitude, *H* the wave height, *T* the wave period, *L* the wave length, *d* the water depth (0.40 m), *Fr* the densimetric Froude number; experiments 1 and 7 were performed without waves as reference cases.

Exp.	*A* [mm]	*H* [mm]	*T* [s]	*L* [m]	*d/L*	*H/L*	*Fr*
1	0	0	-	-	-	-	18.0
2	5.00	10.00	0.50	0.39	1.02	0.026	18.0
3	5.00	10.00	1.00	1.56	0.26	0.006	18.0
4	12.50	25.00	1.00	1.56	0.26	0.015	18.0
5	5.00	10.00	1.50	3.51	0.11	0.003	18.0
6	12.50	25.00	1.50	3.51	0.11	0.007	18.0
7	0	0	-	-	-	-	28.0
8	5.00	10.00	0.50	0.39	1.02	0.026	28.0
9	5.00	10.00	1.00	1.56	0.26	0.006	28.0
10	12.50	25.00	1.00	1.56	0.26	0.015	28.0
11	5.00	10.00	1.50	3.51	0.11	0.003	28.0
12	12.50	25.00	1.50	3.51	0.11	0.007	28.0

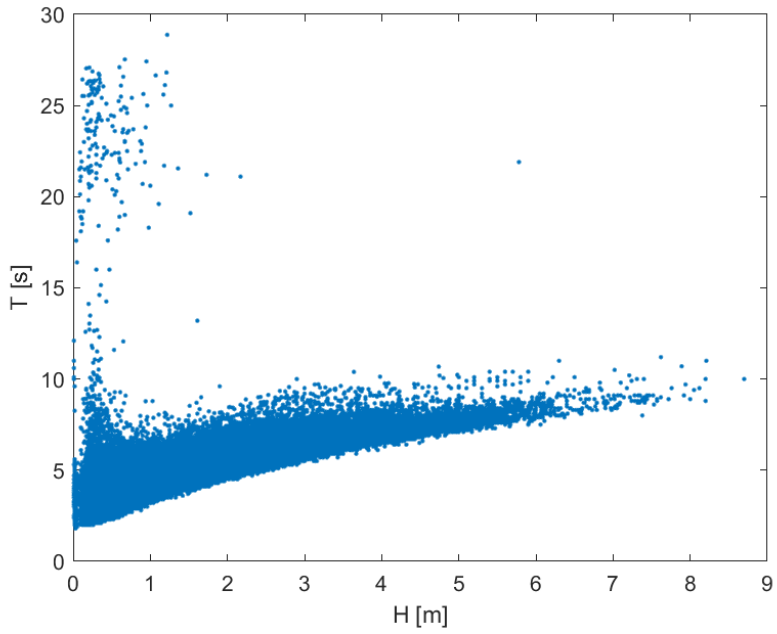

Figure 1. Wave period T versus wave height H recorded by the Alghero wave buoy in the period 2002–2014; data from the Rete Ondametrica Nazionale (Italian National wavemetric System) [37].

In Figures 2 and 3, two instantaneous visualizations of an inclined negatively buoyant jet with $Fr = 28.0$, released respectively in a stagnant and in a wavy environment with $T = 1.00$ s and $A = 12.5$ mm, are shown. High concentrations are indicated by pale grey, low concentrations by dark grey. Figure 2 shows that an inclined NBJ released in a stagnant environment has an ascent region (where the initial momentum prevails on the negative buoyancy) followed by a descent region (where the negative buoyancy prevails). Moreover, the jet luminosity close to the outlet is high (as indicated by the pale grey color) and it tends to reduce along the jet path, pointing out the dilution caused by the entrainment of external fluid into the jet. As a matter of fact, the external fluid has null concentration, so its color is black. Few seconds of this experiment are shown in the movie "Run7_Ferrari_et_al.mp4", available as Supplementary Material. Figure 3 shows the modifications induced on the NBJ (the same of Figure 2) by the waves: Even if these modifications will be discussed in depth in Section 3, it is apparent that this jet, even though it still has an ascent and a descent region, has a different shape and is lower and shorter than the one released in the stagnant environment. Few seconds of this experiment are shown in the movie "Run10_Ferrari_et_al.mp4", available as Supplementary Material.

An image of the background was obtained by recording, before each run, 100 images without the NBJ and computing their point-by-point average. This image of the background was then subtracted from each image with the NBJ, and the resulting images (field of light intensity) were normalized by the grey level measured at the outlet, corresponding to the initial concentration C_0. The subtraction of the background from the images with the jet allows us to remove sources of light not linked to the discharged fluid concentration. The subtraction of the background explains why the cylindrical pipe with the outlet on its wall is visible in Figures 2 and 3 (before the background removal) and not visible in Figures 4–6, Figures 10 and 11 (after the background removal). Under the assumption of ergodicity, the non-dimensional fields of the mean concentration C/C_0 were obtained by time averaging the measured values of C/C_0 on each pixel. The value of C/C_0 is reported in false colors in Figures 4–6, Figures 10 and 11, according to the color bar shown on the left of each Figure (dark red is linked to the highest concentrations, dark blue to the lowest ones). As a consequence, C/C_0 is a measure of the reduction of the mean concentration compared to the outlet concentration C_0: For instance, $C/C_0 = 1$ (dark red) means that the concentration C in that point is the same as C_0 (no dilution), $C/C_0 = 0.5$ (green) means that the concentration C in that point is one half of C_0, $C/C_0 = 0$ (dark blue) means that the concentration C in that point is zero (external fluid not reached by the jet). The x-axis and y-axis are non-dimensionalised by the outlet diameter D, with the origin on the outlet.

The jet axis was assumed as the locus of the concentration maxima on the jet cross-sections (on the non-dimensional mean concentration fields) and it was computed via the iterative procedure described in Ferrari and Querzoli [1]. The stagnant case jet axis was determined on the non-dimensional mean concentration fields shown in Figure 10a for $Fr = 18.0$ and in Figure 4 and Figure 11a for $Fr = 28.0$. This stagnant case jet axis is drawn as a white line in Figures 4–6, Figures 10 and 11 for comparison with the features of the NBJ with the same Fr released into a receiving body affected by regular waves. Moving along the jet axis, the color change from dark red to blue (i.e., from high concentrations to low concentration) highlights the dilution due to the entrainment. As shown in Figures 2 and 4, an inclined NBJ has an ascent and a descent region, so its axis will have a non-symmetrical parabolic-like shape, with the origin coinciding with the outlet (green star in Figure 4, with $X/D = 0$, $Y/D = 0$), a point of maximum height (defined as the highest point reached by the jet axis, with coordinates $X/D = X_h/D$, $Y/D = Y_h/D$) and an impact point (defined as the point where the jet axis reaches again the outlet height, with coordinates $X/D = X_d/D$, $Y/D = 0$). The point of maximum height and the impact point for the stagnant case are drawn, respectively, as a white circle and a white asterisk in Figures 4–6, Figures 10 and 11. The vertical distance between the jet origin and the point of maximum height is defined as the maximum height (vertical orange line in Figure 4) and the horizontal distance between the jet origin and the impact point is defined as the impact distance (horizontal orange line in Figure 4).

The runs in a wavy environment were also analyzed by dividing the wave period in 8 phases equally spaced in time by a $\Delta T = T/8$: phase 1 is taken when the wave trough is above the outlet,

phase 5 corresponds approximately to the moment when the wave crest is above the outlet. In Figure 5 the phase averaged C/C_0 field for phase 1/8 is shown. For the NBjs released into a wave environment, the impact point was measured as the point of maximum height of C/C_0 on the horizontal line $Y/D = 0$ for $X/D > X_h/D$ (i.e., beyond the horizontal coordinate of the point of maximum height; yellow asterisk in Figures 5 and 6), while the point of maximum height for the jet undergoing a bifurcation (see Section 3.1.1 for the phenomenological discussion) was measured in the upper branch of the two branches caused by the bifurcation. In Figures 5 and 6, the point of maximum height is drawn as a magenta circle. In Figure 5, the jet axis of the upper branch as a magenta line, the jet axis of the lower branch as a black line and the jet axis of the descent branch as a yellow line.

See Ferrari and Querzoli, 2010 [1], for more details on the experimental configuration simulating the discharge of inclined NBJs and data elaboration; see Ferrari and Querzoli, 2015 [35] and Ferrari et al., 2016 [40] for more details on the wavemaker system.

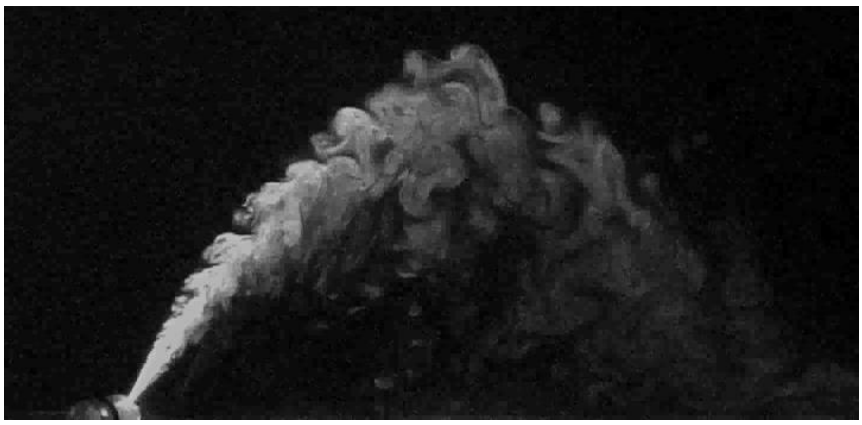

Figure 2. An instantaneous visualization of the concentration field for an inclined negatively buoyant jet with $Fr = 28.0$ and $\theta = 67°$ released into a stagnant receiving body.

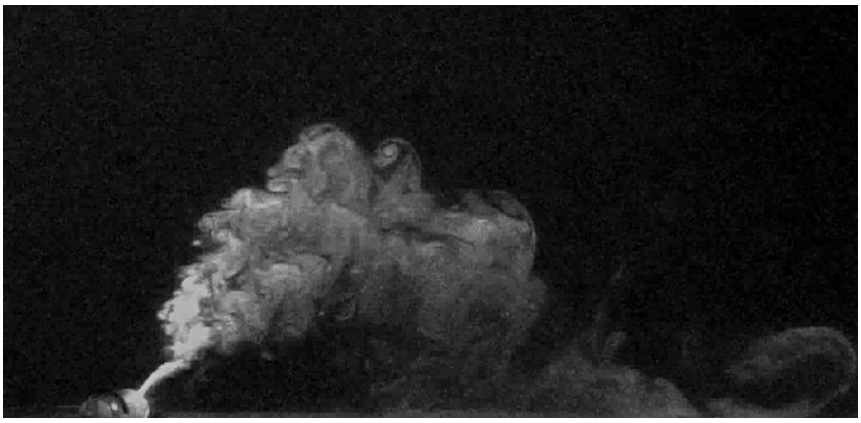

Figure 3. An instantaneous visualization of the concentration field for the same inclined NBJ of Figure 2 released into a receiving body affected by regular waves with $A = 12.5$ mm and $T = 1.00$ s.

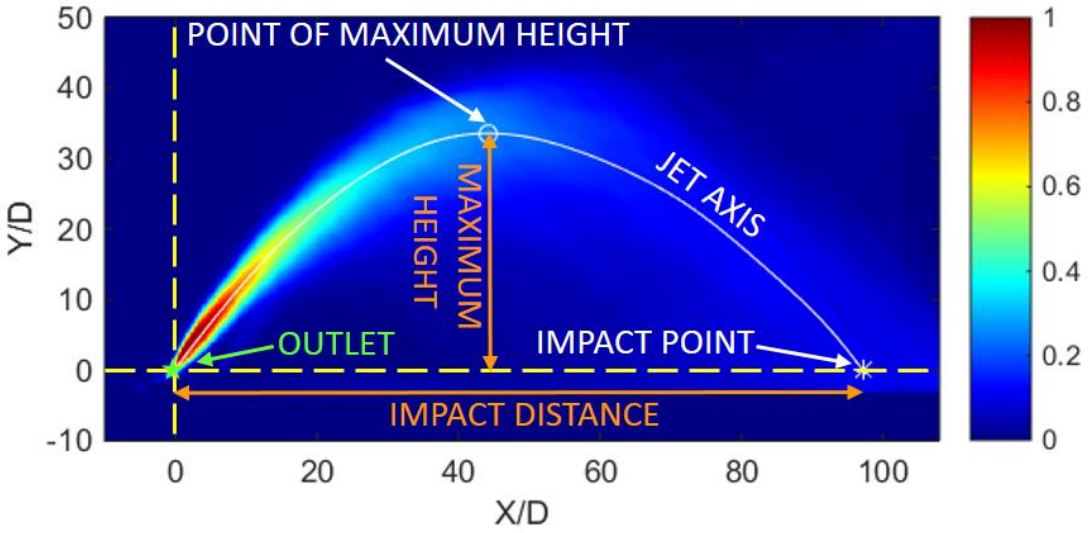

Figure 4. Non-dimensional mean concentration C/C_0 fields for the same inclined NBJ of Figure 2 released into a stagnant receiving body, with the jet geometrical features; the maximum uncertainty in the mean concentration measurement is ±4.41%.

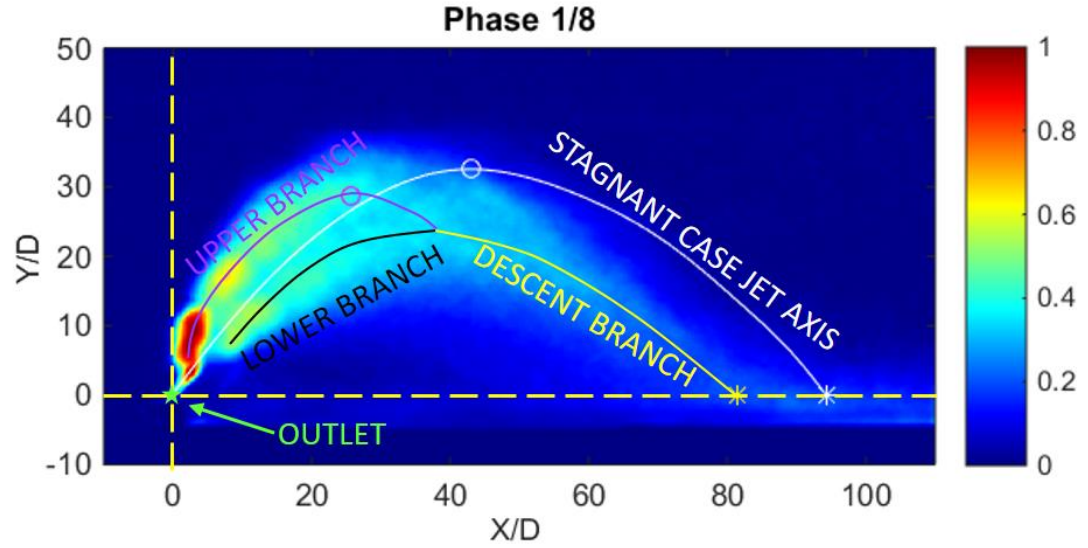

Figure 5. Non-dimensional mean concentration fields for the same NBJ of Figure 3, in phase 1/8, with the jet geometrical features; the maximum uncertainty in the mean concentration measurement is ±4.38%.

3. Results

This section is organized as follows: In Section 3.1, the focus is on the temporal evolution of the phenomenon, so, for each of the eight phases, the mean concentration fields (3.1.1), the maximum height and impact point (3.1.2), and the concentration profiles (3.1.3) are shown; in Section 3.2 the overall mean concentration fields, computed performing the time average on all the images for each run, are presented; eventually, the measured dilutions are reported in Section 3.3.

3.1. Temporal Evolution

3.1.1. Mean Concentration Fields

To better highlight the temporal behaviour of a negatively buoyant jet released upwards with a certain angle to the horizontal when a wave is passing through, in Figure 6 the non-dimensional mean concentration field of an NBJ with Fr = 28.0 subjected to regular waves with T = 1.00 s and A = 12.5 mm has been divided into 8 phases; in addition, to ease the comparison with the stationary case (shown in Figure 4), on each image the stagnant case jet axis (white line) is superimposed. The images of Figure 6 are shown as a movie in "Run10_mean_phase_Ferrari_et_al.mp4", available as Supplementary Material. To highlight the differences between the stationary and the wave case, a white circle and a white asterisk indicate, respectively, the point of maximum height and the impact point for the stationary case, whilst a magenta circle and a yellow asterisk indicate, for each phase, the wave case maximum height point and impact point.

Close to the outlet (X/D = 0, Y/D = 0), the NBJ is deflected upwards or downwards, so it oscillates around the stationary position (pointed out by the white line, i.e., the stationary case jet axis): So in this region the NBJ tends to resist the wave because it tends to preserve its initial direction, as it still retains most of its initial momentum. This behavior is similar to the simple jet one and this region can be identified as the jet deflection region, in agreement with the findings of Chyan and Hwung (1993, [33]) and Mossa (2004 [32]). This oscillation is linked to the position of the wave above the jet which, in turn, is linked to the phase: In phase 1 the wave trough is above the outlet, so there is the largest leftward deflection, while when the wave crest is above the outlet (phase 5), the jet experiences the largest rightward deflection. It is interesting to note that this oscillation is larger upwards than downwards; this is presumably due to the velocity field generated by the interaction between the wave motion (mostly horizontal in that region) and the cylindrical pipe simulating the pipe (visible in Figures 2 and 3). Velocities tend to be higher and directed upwards close to the outlet, whilst they tend to be lower and horizontal in the lower zone. Consequently, the deflection which pushes the jet upwards tends to carry it towards regions with higher velocity and this causes this larger displacement upward.

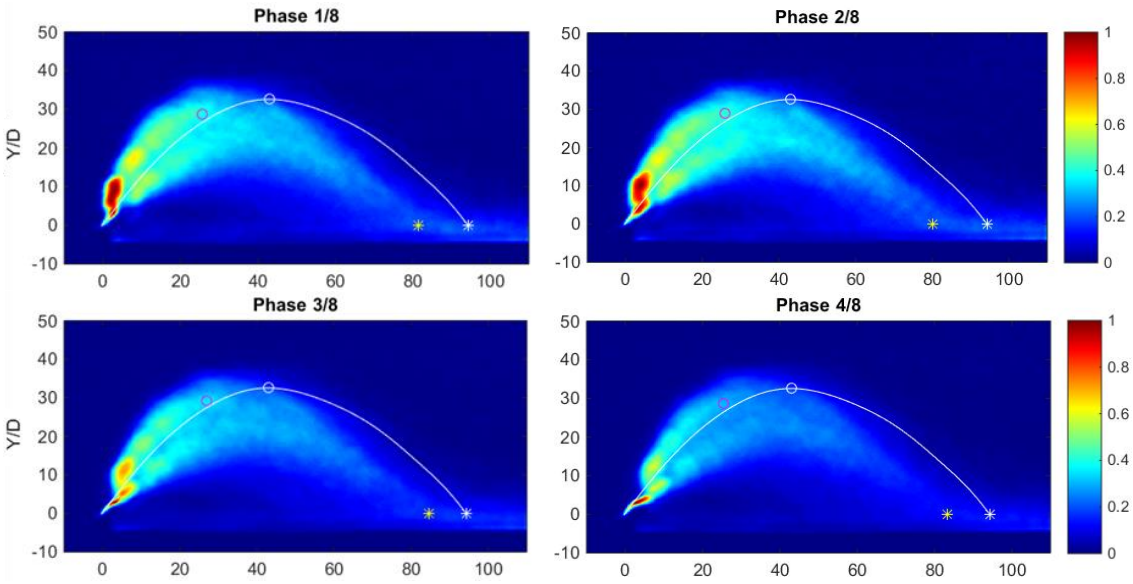

Figure 6. *Cont.*

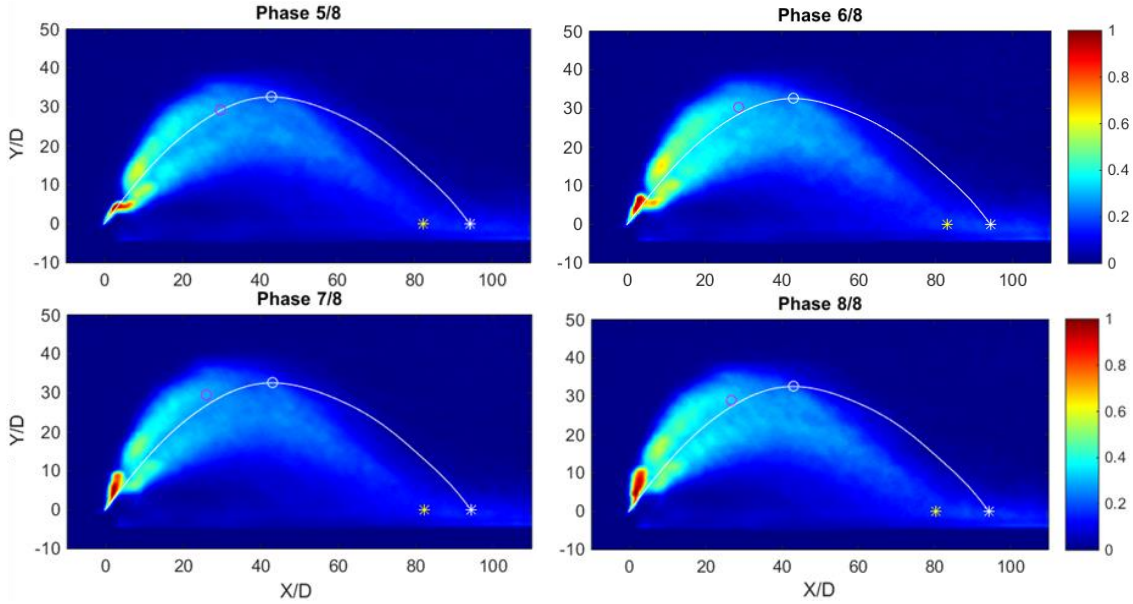

Figure 6. Non-dimensional mean concentration fields for the same NBJ of Figure 3, divided into 8 phases; the white line is the stagnant case jet axis; the maximum uncertainty in the mean concentration measurement is ±4.38%.

Coming back to the observation of Figures 5 and 6, and moving along the jet axis, it is noticeable how, after the jet deflection region, if the wave is intense enough (i.e., with T and A high enough), the NBJ bifurcates; this is the transition region. The jet, slowed down by the enhanced entrainment of low-momentum fluid, is divided into two branches, one mainly higher (magenta line in Figure 5) and one lower (black line in Figure 5) than the stationary jet axis (white line in Figure 5). Eventually, the two branches merge to build up again a single jet flow in the descent branch (yellow line in Figure 5); this is the developed jet region. This bifurcation is sharpened by the fact that the change in the direction is not gradual but, instead, the NBJ in the jet deflection region tends to abruptly move from one extreme to the other.

3.1.2. Geometrical Features

The point of maximum height of the NBJ released into a wavy environment is in the upper branch of the bifurcated jet (magenta asterisk in Figures 5 and 6) and tends to be lower than the same point of the stagnant case jet (white circle in Figures 5 and 6); a similar consideration stands for the impact point (compare the yellow asterisk, i.e., the wave case impact point, with the white asterisk, i.e., the stagnant case impact point, in Figures 5 and 6). For this reason, in Figure 7 the trajectories followed by the points of maximum height for the wave cases (colored lines: blue circles for T = 0.5 s and A = 5.0 mm, green asterisks for T = 1.0 s and A = 5.0 mm, magenta stars for T = 1.0 s and A = 12.5 mm, cyan xs for T = 1.5 s and A = 5.0 mm and red +s for T = 1.5 s and A = 12.5 mm) are compared with the coordinates of the maximum height point for the stagnant case (a single black square, as it does not move in the stagnant case). Similarly, in Figure 8 the oscillation of the impact distances for the wave cases in the various wave phases (colored lines, the same as in Figure 7) are compared with the constant impact distance for the stationary case (black line). In both Figures 7 and 8, the left subfigure refers to the NBJ with Fr = 28 and the right subfigure to the NBJ with Fr = 18.

By looking at Figures 7 and 8, it is possible to note the peculiar behavior of an NBJ released into a wavy environment: The maximum height and the impact distance of the NBJs released in wavy environment are shorter than those of the stationary case for all the different waves tested here. In particular, the ratio between the maximum height for the wave cases and the stagnant case varies from a maximum value of about 0.86 (T = 0.5 s, A = 5.0 mm) to a minimum of about 0.36 (T = 1.5 s,

A = 12.5 mm) for Fr = 28.0, and from a maximum of about 0.83 (T = 0.5 s, A = 5.0 mm) to a minimum of about 0.32 (T = 1.5 s, A = 12.5 mm) for Fr = 18.0.

Moreover, by looking at Figure 7 it is noticeable that the trajectories of the point of maximum height tend to be rotations around a fixed point, even if, in some cases, the closed trajectories are quite flattened. The point of maximum height tends to be lower and closer to the outlet when the wave parameters change: When the wave period T and amplitude A increase, the distance from the stationary position increases. If, on one hand, it is clear that the strongest waves (red +, T = 1.5 s and A = 12.5 mm) have the strongest impact on this phenomenon, on the other the wave period T seems to have the biggest role on the decrease of the maximum height; as a matter of fact, the curves in Figure 7 are sorted by increasing wave period T.

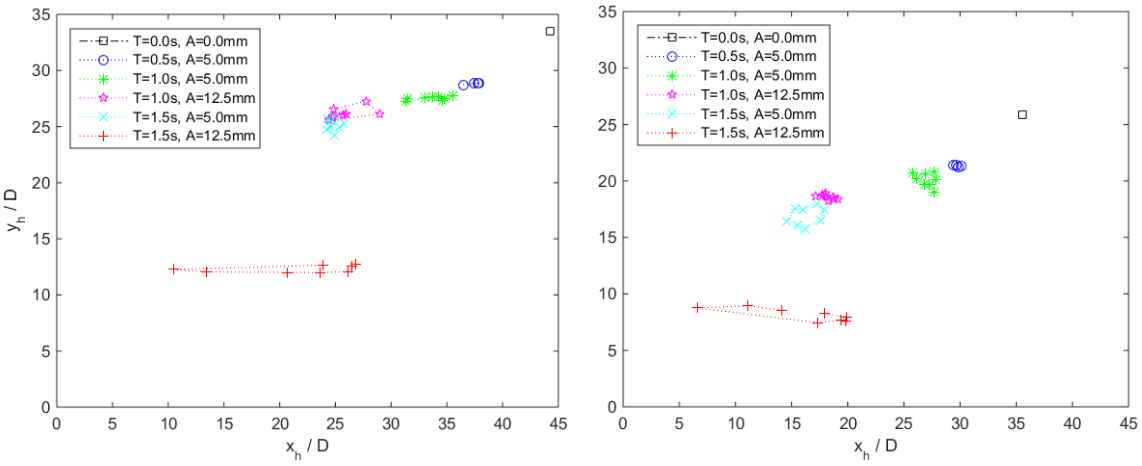

Figure 7. Trajectories of the maximum height points for the NBJs with Fr = 28.0 (**left**) and Fr = 18.0 (**right**) released into a receiving body affected by regular waves (wave parameters in the legend).

The impact point (Figure 8) oscillates around a fixed point which is different from the stationary impact point. Different to the point of maximum height, the impact point seems more influenced by the wave amplitude A; as a matter of fact, in Figure 8, the curves relative to A = 5.0 mm are generally closer to the stationary position than the ones with A = 12.5 mm. The only exception to this rule is the case of T = 0.5 s and A = 5.0 mm for Fr = 28.0 (blue circles on the left of Figure 8); an explanation for this will be given in the Section 3.2. Similar to the maximum height, also the impact distance of the wave cases shows a reduction in size with respect to the stagnant one. In particular, the ratio between the impact distance for the wave cases and the stagnant case varies from a maximum value of about 0.94 (T = 1.5 s, A = 5.0 mm) to a minimum of about 0.51 (T = 1.5 s, A = 12.5 mm) for Fr = 28.0, and from a maximum of about 0.97 (T = 0.5 s, A = 5.0 mm) to a minimum of about 0.54 (T = 1.5 s, A = 12.5 mm) for Fr = 18.0.

In summary, close to the outlet, the NBJ oscillates around the stationary position, as the simple jets; conversely, the NBJ maximum height point rotates around a different position from the stationary maximum height point and the NBJ impact point oscillates around a different position from the stationary impact point.

The reduction of the maximum height and impact distance in the wave cases showed in Figures 7 and 8 confirms the contraction of NBJs when discharged into a wavy environment. This contraction is probably due to the periodic oscillation of the initial direction of the NBJ that causes its bifurcation and a consequent increase of the entrainment; the larger amount of low-momentum external fluid trapped into the NBJ causes a premature slowdown (when compared to the stagnant case).

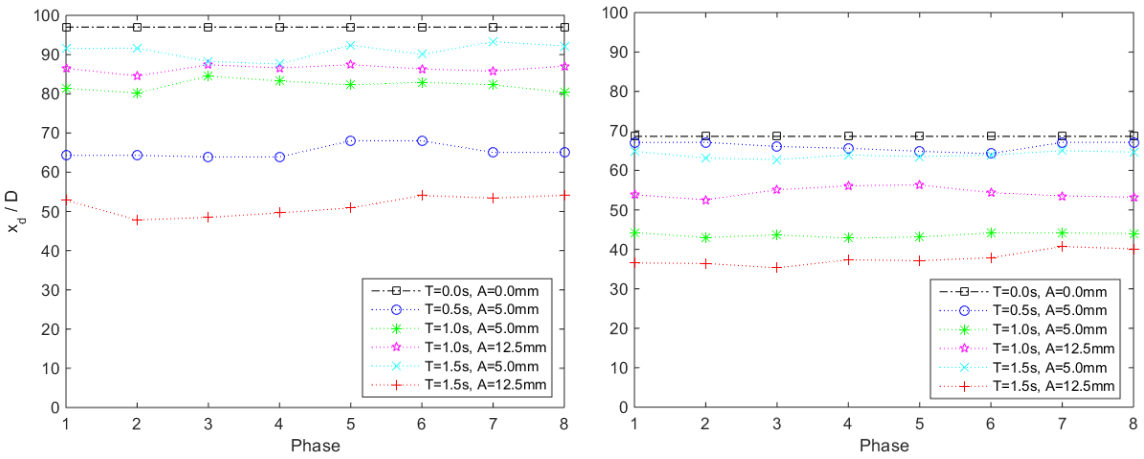

Figure 8. Non-dimensional impact distance x_d/D for the NBJs with Fr = 28.0 (**left**) and Fr = 18.0 (**right**) released into a receiving body affected by regular waves (wave parameters in the legend).

3.1.3. Concentration Profiles

In Figure 9, the cross-sectional profiles of the non-dimensional mean concentration C/C_0 measured on the point of maximum height (a and c, vertical profiles) and on the impact point (b and d, horizontal profiles), in eight different phases of the wave cycle, are shown, for two NBJs with Fr = 28.0 (a and b) and Fr = 18.0 (c and d) released into a receiving body affected by a wave motion with T = 1.00 s and A = 12.5 mm. The different colors highlight the different phases the profiles are measured in. The bimodal distribution of the concentration maxima in Figures 7c and 9a confirms what was previously stated about the bifurcation of NBJs released in a wave environment.

In the impact point, the various profiles have a single peak because here the NBJ is in the developed jet region, where it tends to merge again in a single entity (the yellow line in Figure 5).

The differences among the concentration values in the various phases highlight the different concentration dilutions achieved by the NBJ in the different phases.

3.2. Overall Time Averaged Concentration Fields

In Figures 10 and 11, the mean concentration fields, computed performing the time average over all the images recorded on each experiment and not divided by phases, are shown: Figure 10 concerns the inclined negatively buoyant jets with Fr = 18.0, while Figure 11 concerns the ones with Fr = 28.0. In particular, the Figures 10a and 11a show the inclined NBJs released into a stagnant receiving body, whilst the others (Figures 10b–f and 11b–f) show the inclined NBJs released into a wavy environment.

By comparing the concentration field of the NBJ released into a stagnant environment with those of the NBJs released into a wavy environment, it is apparent how the interaction with the waves causes a contraction of the jet, which tends to be less high and shorter (with a decrease of the maximum height and of the impact distance compared to the stagnant cases, as stated before). This contraction tends to increase as the wave period T and amplitude A increase.

Moreover, for the highest T and A (Figures 10d–f and 11d–f), the distribution of the concentration is bimodal, confirming a bifurcation of the NBJ into two branches, one higher and one lower than the stationary position. These two branches tend to behave as two NBJs released with different angles to the horizontal, to eventually merge when the higher branch falls down on the lower one, causing an increase in the concentration in the lower branch, which is clearly visible in Figures 10f and 11f at $X/D \approx 15$ and $Y/D \approx 10$. This bifurcation, caused by the oscillation of the initial region of the NBJ around the stationary position, becomes more pronounced when the wave amplitude A increases, as it is possible to see from a comparison of the Figure 10d,f (or Figure 11d,f, with A = 12.5 mm) with Figure 10b,c,e (or Figure 11b,c,e, with A = 5.0 mm). If in the first two Figures the bifurcation is more

evident, in the other three it is almost absent or very weak. As a matter of fact, in Figures 10b and 11b the effect of the wave begins to be noticeable only very close to the point of maximum height, where the initial momentum of the NBJ has been almost completely spent. In Figures 10c and 11c, concerning a wave with T = 1.00 s and A = 5.0 mm, the oscillation of the initial region of the NBJ caused by the wave is still present, because the jet widens more than in the stationary case, but it is not sufficient to create the bifurcation. This could suggest that the bifurcation is more linked to high-amplitude waves.

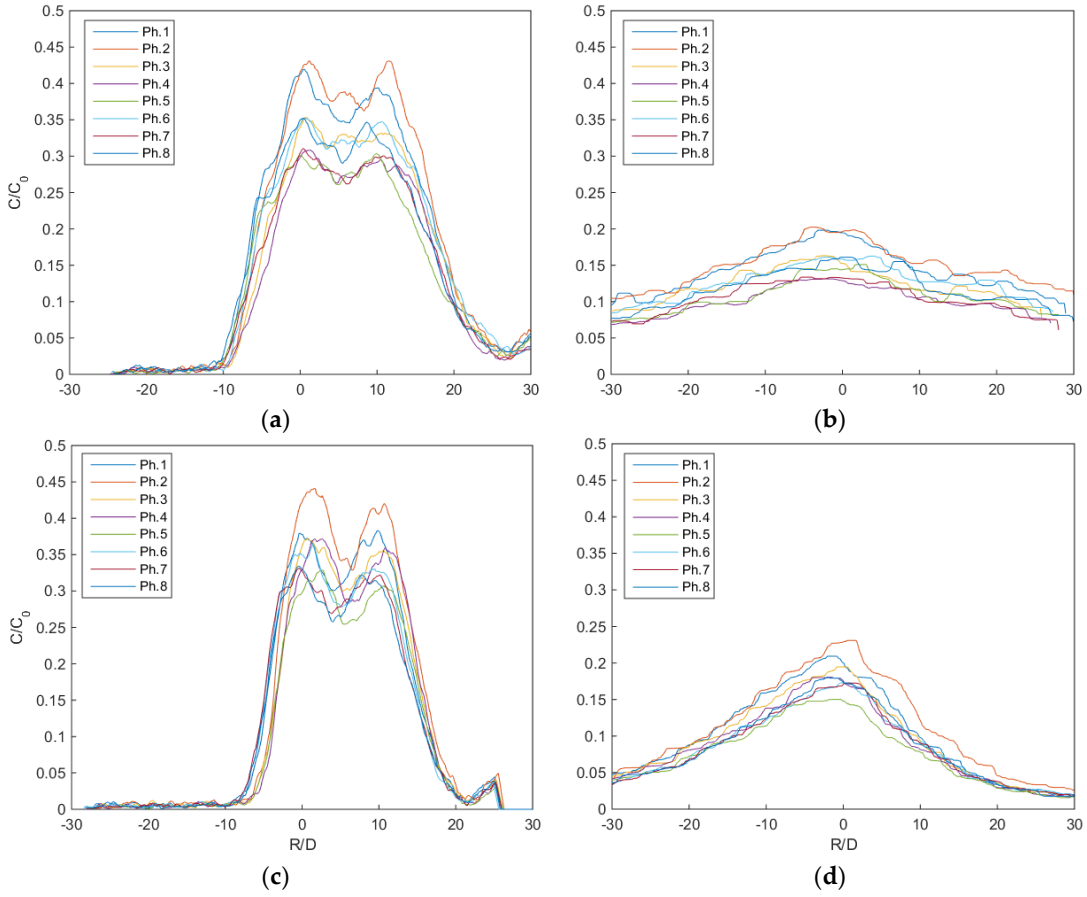

Figure 9. Cross-sectional non-dimensional mean concentration profiles for a NBJ with Fr = 28.0 (**a**,**b**) and for a NBJ with Fr = 18.0 (**c**,**d**) released in a receiving body affected by regular waves with T = 1.00 s and A = 12.5 mm; (a,c) vertical profiles on the point of maximum height; (b,d) horizontal profiles on the impact point; R/D is the non-dimensional span-wise abscissa.

The reduction of the maximum height of the NBJ is mainly caused by the bifurcation. As a matter of fact, because of the strong deflection upwards and downwards imposed by the bifurcation (see Figures 10f and 11f), the jet uses a portion of its initial momentum to return to the initial direction and, consequently, it cannot reach the same height of the stagnant case. When the wave deflects the jet downwards, the trajectory is similar to the one of a NBJ released with a lower angle to the horizontal, i.e., the jet tends to reach a lower maximum height (see Ferrari and Querzoli, 2010, [1]).

The reduction of the impact distance is mainly caused by a combination of the bifurcation and of the rotation of the maximum height point.; the fluid in the lower branch finds the opposition of the oscillating fluid trapped between the bottom and the jet itself, while the fluid in the upper branch, as stated before, falls down on the lower branch, causing an additional mixing and a slowing down of the NBJ.

In Figure 11b, the effect of the wave with T = 0.5 s and A = 5.0 mm on the impact point (compare with Figure 8) can be explained. The wave is too weak to slow down the NBJ enough, so, when the

NBJ comes close to the point of maximum height, it has covered a distance long enough to consume most of its initial momentum and, consequently, it undergoes the rotatory movement imposed by the waves, with an additional stirring that lets the jet fall down almost vertically, with a consequent strong reduction of the impact distance.

In summary, the main effect of the wave amplitude A is the bifurcation of the NBJ, while the one of the wave period T is more linked to the additional stirring, with a rotatory motion, imposed to the transition region of the NBJ. Both these phenomena contribute to consume the initial momentum of the NBJ and to decrease the size of the sea region interested by the NBJ itself. An alternative explanation of these effects of the waves on NBJs could be linked to the Stokes drift. For this reason, we have planned to perform Lagrangian velocity measurements in the future.

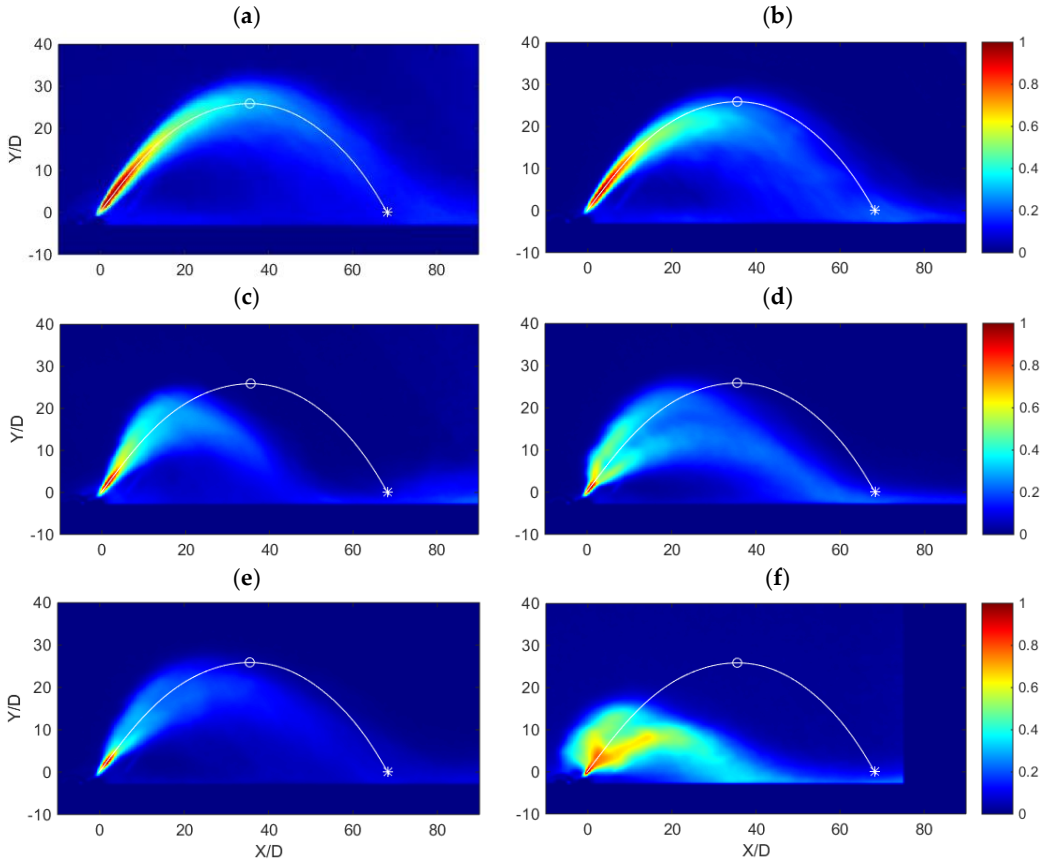

Figure 10. Non-dimensional mean concentration fields for an NBJ with Fr = 18.0 released into a receiving body affected by regular waves with T = 0.0 s and A = 0.0 mm (stagnant case, **a**), T = 0.5 s and A = 5.0 mm (**b**), T = 1.0 s and A = 5.0 mm (**c**), T = 1.0 s and A = 12.5 mm (**d**), T = 1.5 s and A = 5.0 mm (**e**), and T = 1.5 s and A = 12.5 mm (**f**), with the stagnant case jet axis; the maximum uncertainty in the mean concentration measurement is ±3.44% in (**a**), ±3.93% in (**b**), ±3.35% in (**c**), ±3.72% in (**d**), ±3.45% in (**e**), ±3.99% in (**f**).

3.3. Dilution

In order to study the effect of waves on the dilution of inclined negatively buoyant jets, we can define the ratio of the dilution of jets under waves to the dilution of jets in a stagnant environment, if R_{DIL}: if R_{DIL} is higher than one, the waves increase the dilution and vice versa. In Figure 12, R_{DIL} has been plotted versus Fr for all the experiments. The horizontal dotted black line at R_{DIL} = 1 highlights the stagnant case, while, as in the previous Figures, colored lines highlight the wave cases (blue circles for T = 0.5 s and A = 5.0 mm, green asterisks for T = 1.0 s and A = 5.0 mm, magenta stars for T = 1.0 s and A = 12.5 mm, cyan xs for T = 1.5 s and A = 5.0 mm and red +s for T = 1.5 s and A = 12.5 mm). The dilution

is measured, in all the cases, as the inverse of the maximum non-dimensional concentration at the impact point on the overall time-averaged fields, in order to avoid phase variations (see Figure 9b,d).

Figure 12 shows that, differently from what was found by investigations on simple jets or positively buoyant jets, the dilution not always increases for NBJs released in a wavy environment. In particular, the waves with A = 5.0 mm and T = 0.5 s, T = 1.0 s enhance the dilution (R_{DIL} = 1.81 for A = 5.0 mm, T = 0.5 s, Fr = 18.0; R_{DIL} = 1.08 for A = 5.0 mm, T = 1.0 s, Fr = 18.0; R_{DIL} = 1.26 for A = 5.0 mm, T = 0.5 s, Fr = 28.0; R_{DIL} = 1.08 for A = 5.0 mm, T = 1.0 s, Fr = 28.0), whilst the remaining waves (with higher values of A and T) reduce the dilution. The lowest values for R_{DIL} have been measured for the strongest wave (A = 12.5 mm, T = 1.0 s) for both the Fr (R_{DIL} = 0.36 for Fr = 28.0; R_{DIL} = 0.45 for Fr = 18.0).

This result can be explained by two of the effects of the waves on the NBJ: The reduction in size of the sea region interested by the discharge and the bifurcation.

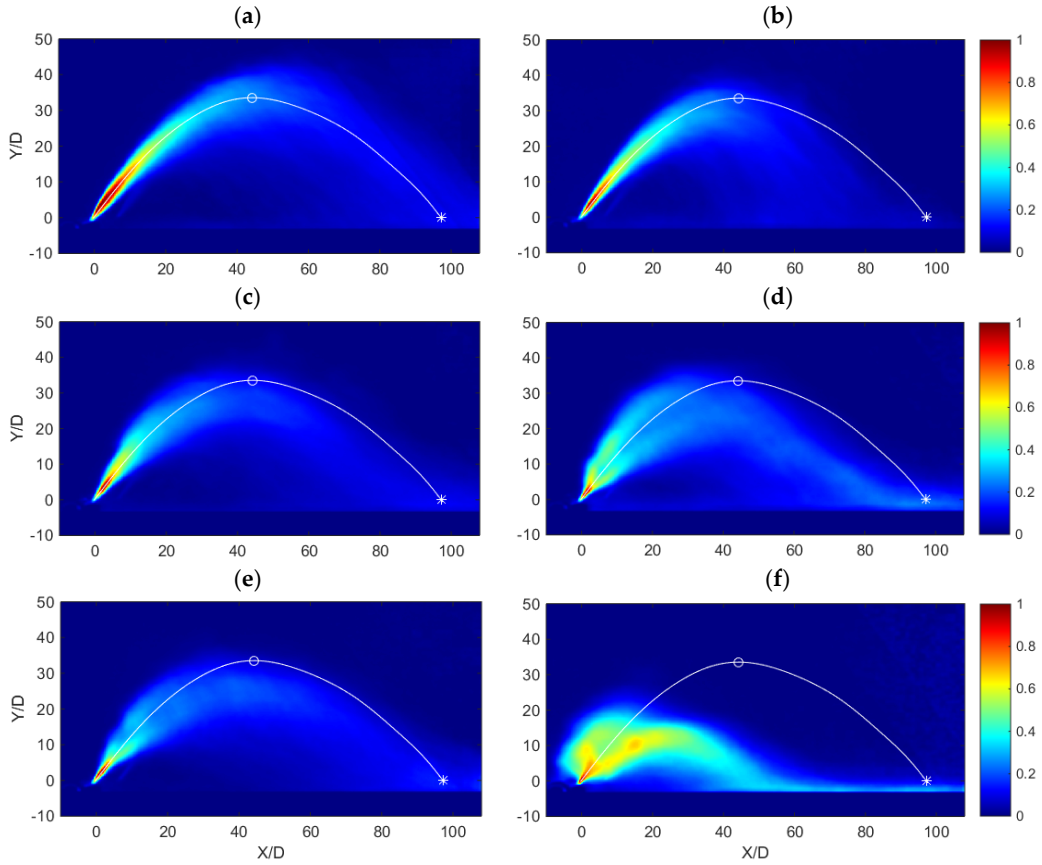

Figure 11. Non-dimensional mean concentration fields for an NBJ with Fr = 28.0 released into a receiving body affected by regular waves with T = 0.0 s and A = 0.0 mm (stagnant case, **a**), T = 0.5 s and A = 5.0 mm (**b**), T = 1.0 s and A = 5.0 mm (**c**), T = 1.0 s and A = 12.5 mm (**d**), T = 1.5 s and A = 5.0 mm (**e**) and T = 1.5 s and A = 12.5 mm (**f**), with the stagnant case jet axis; the maximum uncertainty in the mean concentration measurement is ±4.41% in (**a**), ±4.52% in (**b**), ±4.16% in (**c**), ±4.38% in (**d**), ±4.28% in (**e**), ±4.31% in (**f**).

Because of the contraction, the NBJ is forced by the waves to remain in a smaller region compared to the stagnant case, so the path available for mixing is decreased and this can reduce (or even cancel) the additional stirring caused by the rotation. Moreover, if the NBJ is forced into a smaller region, it will tend to re-entrain some jet fluid instead of entraining external fluid.

The bifurcation has a conflicting role: On one hand, it increases the surface available for entrainment, but, on the other hand, the lower boundary of the upper branch and the upper boundary

of the lower branch tend to exchange jet fluid between themselves and not to entrain external fluid, reducing the dilution. Moreover, as shown in the previous subsections, the upper branch tends to fall down over the lower one, causing an increase in concentration along the path of the wave case NBJ.

The authors cited in the introduction found that discharging a horizontal NBJ or a simple jet in the opposite direction to the wave propagation increases in size the region occupied by the jet and, as a consequence, its dilution. In the present case, an inclined NBJ (in particular with the strongest waves) experiences, as previously seen, a reduction in size of the region occupied by the jet in comparison with the stagnant case which, consequently, leads to a lower dilution.

For these reasons, the waves that cause the worst dilutions are the ones with A = 12.5 mm. On the contrary, the two waves with A = 5.0 mm and T = 0.5 s, T = 1.0 s enhance the dilution, because the rotation imposed by the waves on the NBJs is intense enough to compensate their contraction (which, anyway, is smaller than in the other cases).

In summary, the peculiar nature of inclined NBJs, which tend to behave in a limited region of space and cannot reach an asymptotic state like some simple or positively buoyant jets, leads to the conclusion that the wave motion not always enhances their dilution. In particular, the strongest waves tested in the present work tend to reduce the dilution, whilst the weakest ones tend to enhance it.

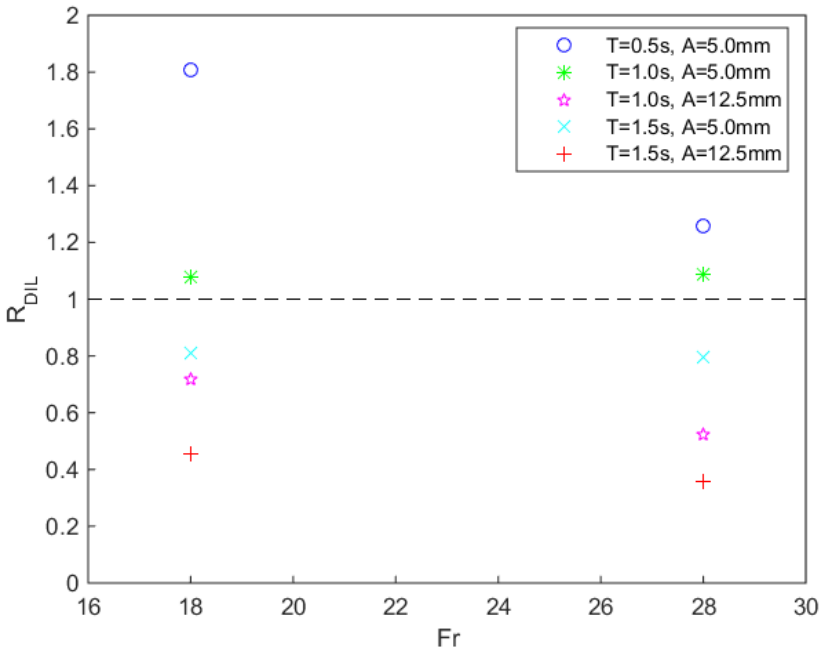

Figure 12. R_{DIL} versus Fr; R_{DIL} is the ratio of the dilution of NBJs under waves to the dilution of jets in stagnant environment; (wave parameters in the legend).

4. Conclusions

With the target to measure the modifications that regular waves induce on the geometrical features and on the dilution of inclined negatively buoyant jets, we have carried out an experimental campaign on a laboratory model of a submerged outfall discharging brine under some typical conditions of the Mediterranean Sea. In particular, the concentration fields were measured via a non-intrusive and full-field light-induced fluorescence technique.

Differently from simple jets under regular waves, in inclined negatively buoyant jets the point of maximum height rotates and the impact point oscillates around a fixed position, which is different from that of the stationary case. Both the maximum height and the impact distance are smaller than the corresponding ones without waves and are more influenced by the wave amplitude. The oscillation of the initial region of the negatively buoyant jet causes a bifurcation, more pronounced when the

wave amplitude A increases. As a consequence of the previous two effects, the region interested by the discharge is reduced in size by the wave action.

Differently from simple or positively buoyant jets, the dilution of inclined negatively buoyant jets is not always enhanced by waves. Specifically, the strongest waves tested in the present work tend to reduce the dilution, whilst the weakest ones tend to enhance it. As usually the stagnant receiving body case is considered the worst one for dilution, designers should pay particular attention in the case of dense discharges, because in regions often affected by strong waves the wavy receiving body conditions might be more critical for dilution and, consequently, for environmental preservation.

Supplementary Materials: The following are available online at www.mdpi.com/10/6/726/s1, The movie "Run7_Ferrari_et_al.mp4" depicts few seconds of Run 7 of Table 1, i.e., a NBJ with Fr = 28 released in a stagnant environment. The movie "Run10_Ferrari_et_al.mp4" depicts few seconds of Run 10 of Table 1, i.e., the same NBJ of the previous movie but released into a receiving body affected by regular waves with A = 12.5 mm and T = 1.00 s. The movie "Run10_mean_phase_Ferrari_et_al.mp4" depicts the non-dimensional mean concentration fields for the same NBJ of the previous movie, divided into 8 phases; the white line is the stagnant case jet axis, the white circle is the stagnant case point of maximum height and the white asterisk is the stagnant case impact point.

Author Contributions: S.F. and G.Q. conceived, designed and performed the experiments; S.F., M.G.B. and G.Q. analyzed the data and wrote the paper.

Acknowledgments: The present research was funded by the University of Cagliari. The authors very much appreciate all the help provided by Mr. Antonio Mascia.

Conflicts of Interest: The authors declare no conflict of interest.

References

1. Ferrari, S.; Querzoli, G. Mixing and re-entrainment in a negatively buoyant jet. *J. Hydraul. Res.* **2010**, *48*, 632–640. [CrossRef]
2. Qiao, Q.S.; Choi, K.W.; Chan, S.N.; Lee, J.H.W. Internal hydraulics of a chlorine jet diffuser. *J. Hydraul. Eng.* **2017**, *143*, 06017022. [CrossRef]
3. Bashitialshaaer, R.; Larson, M.; Persson, K.M. An experimental investigation on inclined negatively buoyant jets. *Water* **2012**, *4*, 720–738. [CrossRef]
4. Bashitialshaaer, R.; Persson, K.M.; Larson, M. New criteria for brine discharge outfalls from desalination plants. *Environ. Sci. Eng.* **2015**, *149*, 451–467. [CrossRef]
5. Seo, I.W.; Song, C.G. Dispersion of negatively buoyant effluent jetted from ORV. *KSCE J. Civ. Eng.* **2015**, *19*, 1164–1173. [CrossRef]
6. Christodoulou, G.C.; Papakonstantis, I.G.; Nikiforakis, I.K. Desalination brine disposal by means of negatively buoyant jets. *Desalin. Water Treat.* **2015**, *53*, 3208–3213. [CrossRef]
7. Oliver, C.J.; Davidson, M.J.; Nokes, R.I. Removing the boundary influence on negatively buoyant jets. *Environ. Fluid Mech.* **2013**, *13*, 625–648. [CrossRef]
8. Geyer, A.; Phillips, J.C.; Mier-Torrecilla, M.; Idelsohn, S.R.; Oñate, E. Flow behaviour of negatively buoyant jets in immiscible ambient fluid. *Exp. Fluids* **2012**, *52*, 261–271. [CrossRef]
9. Papakonstantis, I.G.; Christodoulou, G.C.; Papanicolaou, P.N. Inclined negatively buoyant jets 1: Geometrical characteristics. *J. Hydraul. Res.* **2011**, *49*, 3–12. [CrossRef]
10. Papakonstantis, I.G.; Christodoulou, G.C.; Papanicolaou, P.N. Inclined negatively buoyant jets 2: Concentration measurements. *J. Hydraul. Res.* **2011**, *49*, 13–22. [CrossRef]
11. Crowe, A.T.; Davidson, M.J.; Nokes, R.I. Maximum height and return point velocities of desalination brine discharges. In Proceedings of the 18th Australasian Fluid Mechanics Conference, Launceston, Australia, 3–7 December 2012.
12. Crowe, A.T.; Davidson, M.J.; Nokes, R.I. Velocity measurements in inclined negatively buoyant jets. *Environ. Fluid Mech.* **2016**, *16*, 503–520. [CrossRef]
13. Besalduch, L.A.; Badas, M.G.; Ferrari, S.; Querzoli, G. Experimental studies for the characterization of the mixing processes in negative buoyant jets. *Eur. Phys. J. WoC* **2013**, *45*, 01012. [CrossRef]
14. Besalduch, L.A.; Badas, M.G.; Ferrari, S.; Querzoli, G. On the near field behavior of inclined negatively buoyant jets. *Eur. Phys. J. WoC* **2014**, *67*, 02007. [CrossRef]

15. Malcangio, D.; Ben Meftah, M.; Mossa, M. Physical modelling of buoyant effluents discharged into a cross flow. In Proceedings of the 2016 IEEE Workshop on Environmental, Energy, and Structural Monitoring Systems, Bari, Italy, 13–14 June 2016. [CrossRef]
16. Hajikandi, H.; Barjastehmaleki, S. Negatively buoyant jets at low froude numbers in a co-flow. *Proc. Inst. Civ. Eng. Water Manag.* **2015**, *168*, 129–138. [CrossRef]
17. Lai, C.C.K.; Lee, J.H.W. Initial mixing of inclined dense jet in perpendicular crossflow. *Environ. Fluid Mech.* **2014**, *14*, 25–49. [CrossRef]
18. Yang, Z.-H.; Huai, W.-X.; Dai, H.-C. Experimental investigation into hot water slot jets with negatively buoyancy in cross flow. *J. Hydrodyn.* **2005**, *17*, 412–417.
19. Davies, P.A.; Käse, R.H.; Ahmed, I. Laboratory and numerical model studies of a negatively-buoyant jet discharged horizontally into a homogeneous rotating fluid. *Geophys. Astro Fluid* **2001**, *95*, 127–183. [CrossRef]
20. Davies, P.A.; Ahmed, I. Laboratory studies of a round, negatively buoyant jet discharged horizontally into a rotating homogeneous fluid. *Fluid Dyn. Res.* **1996**, *17*, 237–274. [CrossRef]
21. Stancanelli, M.; Musumeci, R.E.; Foti, E. Dynamics of gravity currents in the presence of surfacewaves. *J. Geophys. Res. Ocean.* **2018**. [CrossRef]
22. Bas, B.; Sedat Kabdasli, M.; Nur Erturk Bozkurtoglu, S.; Zafer Seker, D. Effect of wave direction on discharged brine dilution. *Fresenius Environ. Bull.* **2012**, *21*, 3093–3100.
23. Lin, J.F.; Hsiao, S.C.; Hsu, T.W.; Chang, K.A. Experimental study of a negatively buoyant horizontal jet in wave environment. *Proc. Int. Conf. Offshore Mech. Arct. Eng.* **2011**, *6*, 191–198. [CrossRef]
24. Lin, J.F.; Hsiao, S.C.; Hsu, T.W.; Chang, K.A. Buoyancy effect on turbulent round jet under regular waves. *J. Waterw. Port. Coast. Ocean. Eng.* **2013**, *139*, 190–208. [CrossRef]
25. Chin, D.A. Influence of surface waves on outfall dilution. *J. Hydraul. Eng.* **1987**, *113*, 1006–1018. [CrossRef]
26. Sharp, J.J. The effects of waves on buoyant jets. *Proc. Inst. Civ. Eng.* **1986**, *81*, 471–475.
27. Xu, Z.; Chen, Y.; Tao, J.; Pan, Y.; Sowa, D.M.A.; Li, C.-W. Three-dimensional flow structure of a non-buoyant jet in a wave-current coexisting environment. *Ocean. Eng.* **2016**, *116*, 42–54. [CrossRef]
28. Xu, Z.S.; Chen, Y.P.; Tao, J.F.; Pan, Y.; Zhang, C.K.; Li, C.W. Modelling of a non-buoyant vertical jet in waves and currents. *J. Hydrodyn.* **2016**, *28*, 778–793. [CrossRef]
29. Hsiao, S.C.; Hsu, T.W.; Lin, J.-F.; Chang, K.A. Mean and turbulence properties of a neutrally buoyant round jet in a wave environment. *J. Waterw. Port. Coast. Ocean. Eng.* **2011**, *137*, 109–122. [CrossRef]
30. Chang, K.A.; Ryu, Y.; Mori, N. Parameterization of neutrally buoyant horizontal round jet in wave environment. *J. Waterw. Port. Coast. Ocean. Eng.* **2009**, *135*, 100–107. [CrossRef]
31. Ryu, Y.; Chang, K.A.; Mori, N. Dispersion of neutrally buoyant horizontal round jet in wave environment. *J. Hydraul. Eng.* **2005**, *131*, 1088–1097. [CrossRef]
32. Mossa, M. Experimental study on the interaction of non buoyant jets and waves. *J. Hydraul. Res.* **2004**, *42*, 13–28. [CrossRef]
33. Chyan, J.M.; Hwung, H.H. On the interaction of a turbulent jet with waves. *J. Hydraul. Res.* **1993**, *31*, 791–810. [CrossRef]
34. Chyan, J.; Hwung, H.; Chang, Y. Wave effects on the mean flow characteristics of turbulent round jets. In *Environmental Hydraulics*; Lee, J., Cheung, Y., Eds.; Balkema: Rotterdam, The Netherlands, 1991.
35. Ferrari, S.; Querzoli, G. Laboratory experiments on the interaction between inclined negatively buoyant jets and regular waves. *Eur. Phys. J. WoC* **2015**, *92*, 02018. [CrossRef]
36. Von Ellenrieder, K.D.; Dhanak, M.R. Hydromechanics. In *Springer Handbook of Ocean Engineering*; Dhanak, M.R., Xiros, N.I., Eds.; Springer: New York, NY, USA, 2016; ISBN 978-3-319-16648-3.
37. RON-Rete Ondametrica Nazionale (Italian National wavemetric System). Available online: http://dati.isprambiente.it/dataset/ron-rete-ondametrica-nazionale/ (accessed on 14 March 2018).
38. Troy, C.D.; Koseff, J.R. The generation and quantitative visualization of internal breaking waves. *Exp. Fluids* **2005**, *38*, 549–562. [CrossRef]
39. Sutton, J.A.; Fisher, B.T.; Fleming, J.W. A laser-induced fluorescence measurement for aqueous fluid flows with improved temperature sensitivity. *Exp. Fluids* **2008**, *45*, 869–881. [CrossRef]

40. Ferrari, S.; Badas, M.G.; Querzoli, G. A non-intrusive and continuous-in-space technique to investigate the wave transformation and breaking over a breakwater. *Eur. Phys. J. WoC* **2016**, *114*, 02022. [CrossRef]
41. Bendat, J.S.; Piersol, A.G. *Random Data: Analysis and Measurement Procedures*, 4th ed.; Wiley and Sons: Hoboken, NJ, USA, 2010; pp. 1–640. ISBN 978-0-470-24877-5.